STUDY FOR LAND SURFACE PROPERTIES WITH ALOS PALSAR

PI No. 017

PI: Guo huadong, CI: Table II

Center for Earth Observation & Digital Earth, Chinese Academy of Sciences, No.9 Dengzhuang South Road, Haidian District, Beijing, P. R. China
Tel: 86-10-82178000, Fax: 86-10-82178009, Email: hdguo@ceode.ac.cn

1. ABSTRACT

China is a country with vast land and various kinds of land surface. Study for land surface properties with the advanced ALOS/PALSAR system will contribute to solving scientific problems addressing many environmental issues in a broad range of Earth science disciplines. Owing to the rapid economic development and population expansion in the past two decades, many environmental problems are increasingly serious, such as farmland decreasing, soil erosion increasing, deforestation, and desertification. With the advanced ALOS/PALSAR and other sensors as supplemental data acquisition sources, it is possible to conduct research works addressing many environmental issues related to land surface properties. This report will give results we obtained in different areas, such as glacier movement, earthquake, Great wall study and etc.., all these study show powerful potential of ALOS sensors in environment change study.

.

2. INTRODUCTION

Global environmental change has brought widespread attention all over the world. Global Environmental Change is giving big impact to human society, and it has attracted greatest attentions of various countries and becoming one major issue for researchers. The report is focus on the environment change monitoring using ALOS PALSAR, several aspects are studied. An pixel offset track method was implemented and the Muztagh glacier was studied and the velocity of the glacier is obtained. An improved HIS fusion method and PC fusion method which are pixel-level fusion were implemented for image fusion processing. The skeleton extraction method that can extract spatial location of the linear object automatically was completed, and was used to automatically extract accurate spatial location of the Ming Great Wall based on fused image of PC method. The new roll invariant target scattering decomposition-Touzi target scattering decomposition has been completed. An Genetic Algorithm for the inversion of the surface parameters retrieve was completed, use this method the inverted parameters such as RMSH Correlation Length and the Soil moisture content (in volume) can be obtained.

InSAR process flow for PALSAR was finished and Chengdu and Yushu earthquake data were analyzed. We obtained some good result.

3. GLACIER MOVEMENT MONITORING

Muztagh glacier located in Xinjiang Province, the geographical position is N38°00 ' ~38°30 ', E74°50 ' ~75°40 '. The area of this glacier reduced 1.11% during 1965 and 2001. The peak of the mountain is 7546 meters, the largest glacier is located in east part of the area, called Kekeshayi glacier, the area is about 86.5 km^2. It is the most important water supply of Tarim basin. The velocity of the glacier is an important parameter of glacier, in this study we design an offset track method and obtain the velocity of the glacier. The work flow is as Fig.1.

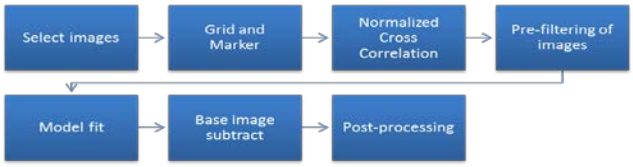

Fig.1 work flow of offset track method

We obtain two PALSAR image of Jan. 2009 and March 2009, using offset track method we obtained the 2D velocity map of kekeshayi glacier, the results show that the largest velocity is about meters per month.

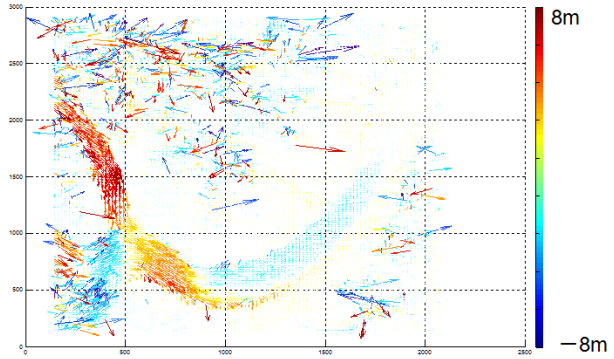

Fig.2 2D velocity map of KeKeshayi glacier

For intuitionistic know the velocity and the topography, the 2D velocity map is overlaid on a DEM, the result shows in Fig.3. From Fig.3 we could see strong relationship between topography and velocity of the glacier.

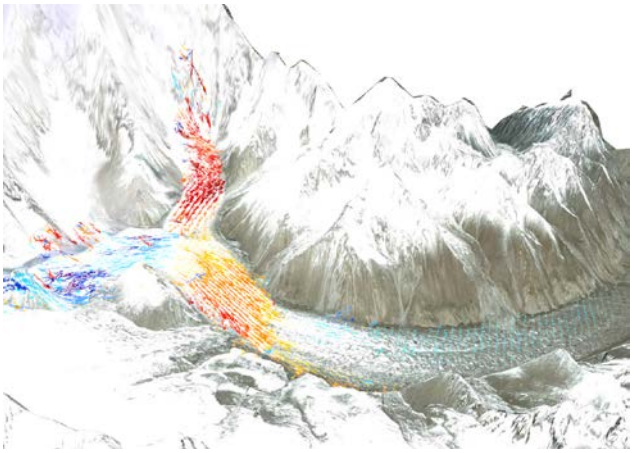

Fig.3 3D velocity map of KeKeshayi glacier

4. YUSHU EARTHQUAKE CO-SEISMIC DEFORMATION FIELD

Two PALSAR images (see TABLE I) taken on January 15 2010 and April 17, 2010, both with the FBS (fine beam single) mode, are used to generate the co-seismic D-InSAR image. The perpendicular baseline is 700.5m around the middle of the image. These images are acquired from the ascending orbit, thus the line-of-sight (LOS) is as shown in the Fig 1. The incidence angle is 34.3°from the vertical.

TABLE I. PALSAR PARAMETERS FOR SAR INTERFEROMETRY

Date	Track	Frame	Perpendicular Baseline (m)	Temporal baseline (d)
JAN.15,2010	487	650	700.5	92
APR.17,2010	487	650		

As can be seen in Fig.4, interferometric signal shows that there is a linear feature trending southeast-northwest, demonstrating active deformation in this area. This southeast-northwest trending deformation zone is along the Yushu-Ganzi fault and about 40km wide. There are three color cycle fringes could be counted in both side of the earthquake fault. One color cycle corresponding half of the wavelength is about 11.8cm along the LOS direction.

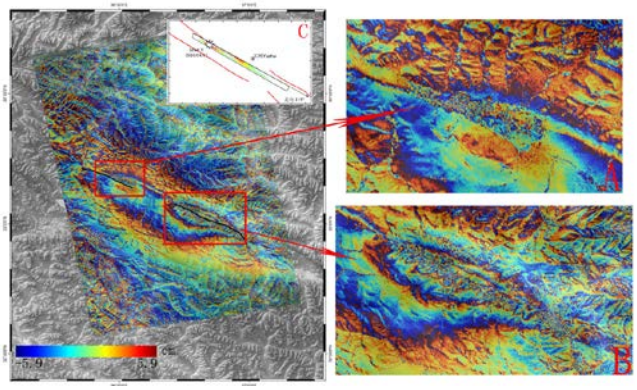

Fig.4. Co-seismic D-InSAR interferogram map.A and B are the epicenters corresponding to the instrumental-epicenter and macro-epicenter. Inset C is the simulation result from China seismological Bureau.

To illustrate the deformation trend, three profiles cross the fault are extracted from the interferogram (Fig.5 red lines).

The mm' profile (Fig.6) runs north-south across the eastern extension of the fault and shows a great difference of up to more than 40cm in the deformation, with the northern part of fault moving away in LOS direction and oppositely in the southern part of the fault. The profile nn' shows a clear uplift trend in the northern part of fault and subsidence trend in the southern part of the fault. The profiles of oo' and hh' also show the same trend as the profiles of mm' and nn'. But hh' has a small change rate compared to that of the other three profiles with sudden change. The signal on the deformation center area is lost because of low coherence due to heavily change of the surface.

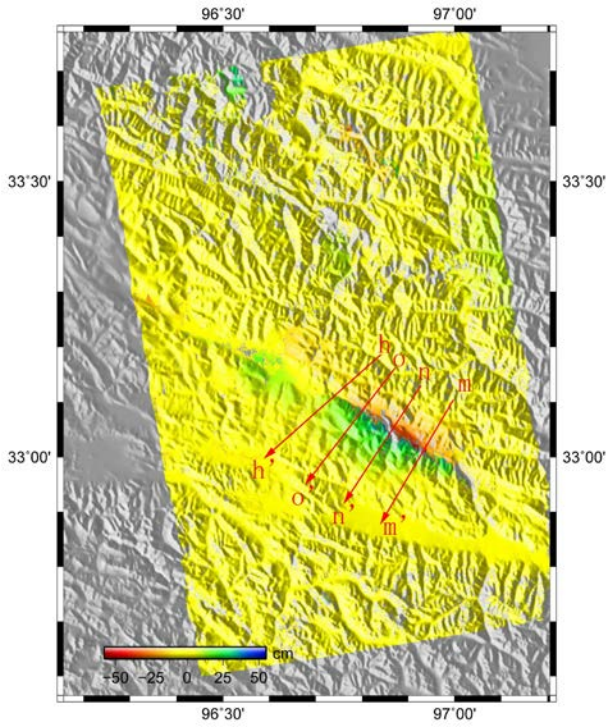

Fig.5. Co-seismic unwrapped interferogram map.Four profiles cross the heavy change part of fault.

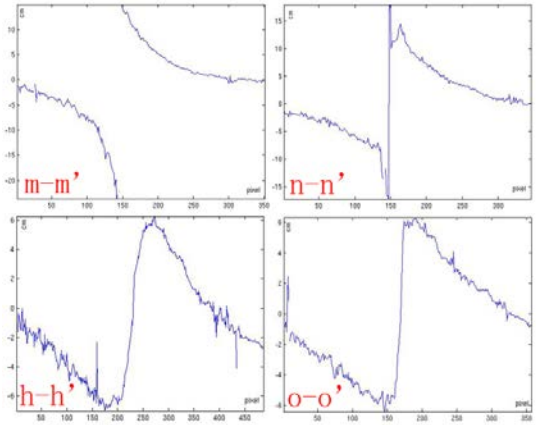

Fig.6 Profiles across the earthquake fault.

The main goal of using the D-InSAR is to investigate the surface deformation of the region of the earthquake and to analysis the relation between the observed deformation field and the discrete fault. It is discovered from D-InSAR

results that there are two deformation centers, corresponding to two epicentres, along the Yushu-Ganzi fault which occurred the earthquake (Fig.4). The Yushu city, which suffering the heavy damage due to the earthquake, is prone to seismicity corresponding to one epicenter of earthquake.

The reduction of coherence is generally due to the change in surface properties, the low coherence part is due to the change of surface cover between master and slave images with differently acquired time. The area of low coherence near the fault region, where is a lake, is likely due to destruction by the strong motion. The seismic hazard for producing disasters is highly related to geological, physiographical, and tectonics factors such as population density, regional deformation, construction code in the affected area and soil and rock types among others; and is closely correlated with various intensities of earthquakes and shocks

Uncertainties of LOS displacements inferred from the interferogram are hard to assess. The error and its spatial correlation in InSAR data are controlled by various factors, including the baseline length of satellite orbit pair and atmospheric disturbance, which the shorter of perpendicular baseline the more accuracy of the deformation in LOS direction, but how they contribute to the error is partly still enigmatic. We neglect the atmospheric contribution in this work to simplify the calculation and because the deformation signal is so large that the atmospheric contribution does not play a significantly role in the finally data analysis.

From the final interferogram, the overall trend of the earthquake deformation is 120º from the north. The nearer is from the Yushu-Ganzi surface fault zone, the greater the ground deformation is deduced in the interferogram. From the fringe density of the both sides, the change gradient of the north part is much greater than that of the south part of the Yushu-Ganzi fault. The largest deformation detected by the D-InSAR approach is around the 30.0ºN, 96.8ºE along the fault zone. The largest deformation along the radar look sight is up to 57.8cm. The result derived from the interferogram agrees with the maximum deformation center of field investigation. The surface uplift and sinistral strike-slip movement of the Yushu-Ganzi fault presents opposite contributions to the deformation along the LOS direction. The vertical motion and sinistral strike-slip motion could not be inverted from the only deformation along the LOS direction directly.

5. DETECTING THE GREAT WALL IN THE NINGXIA AND SHANXI PROVINCE

How to trace the Great Wall which had disappeared from the earth's surface, and how to further research on the environment around it based on the spatial location of the Great Wall which has been detected, first of all, we must detect the Great Wall. So we must choose an optimum way to locate exactly the spatial location of the Great Wall. In our study, we chose the ALOS PALSAR (L-HH) as our means of detection, assisting with optical image Landsat ETM+ by multi-sensors remote sensing image fusion.

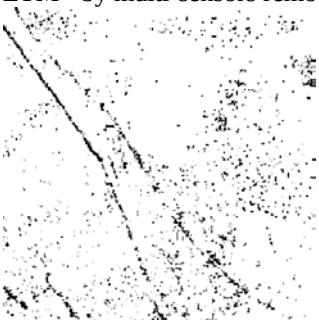

a.binary image based on fused image

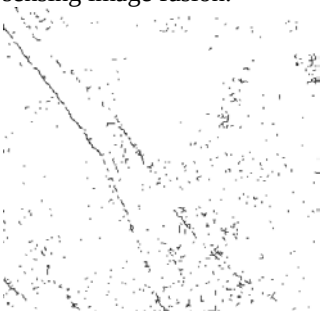

b. the extracting information by skeleton method

c. the accurate location of the Ming Great Wall

Fig.7 the procedure chart of extracting information of the Ming Great Wall using skeleton method

It is different from conventional information extraction of linear object based on visual interpretation; the skeleton extraction method could extract spatial location of the linear object automatically. So the skeleton method was used to automatically extract accurate spatial location of the Ming Great Wall based on fused image of PC method. But road and the Ming Great Wall which are two linear objects in extraction image are easy to confuse, so spectrum threshold of road and the Ming Great Wall which was extracted from fused image by respectively choosing 10 sampling points was used to distinguish the Ming Great Wall from other linear objects. The process of extracting information of the Ming Great Wall using skeleton method is showed in Fig 7.

In our study area, there are two SAR image, they are SIR-C and ALOS Palsar respectively. In the imaging region, Guo Huadong found some detection results about the Ming Great Wall based on SIR-C (R：L-HH、G：L-HV、B：C-HV). For example, there are three Great Wall Nearly parallel in this region, two of them built in Ming dynasty were respectively called as the first wall and the second wall, and one of them built in Sui dynasty was called as the Sui Great Wall. The position of the first wall and the Sui Great Wall is very closely in space, and the second wall is much far away from the first wall's north. Their spatial locations are showed in Fig 8.

Fig.8 the detection result of the Great Wall in our study area based on SIR-C (L-HH)

But the detection result of the Great Wall displayed in ALOS PALSAR is different from the SIR-C's in same study area with same band (L band) and same polarization mode (HH). The detection result of the Great Wall displayed in ALOS PALSAR is showed in Fig 9-a and Fig 9-b.

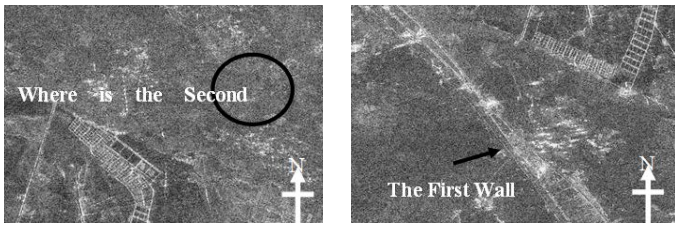

a b

Fig.9 the detection result of the Great Wall in our study area based on ALOS Palsar (L-HH)

For explaining this phenomenon, firstly we should unify their resolution to 15 meter because they have different spatial resolutions that respectively are 25 meter and 10 meter; secondly we should adjust their gray value into the same distribution scope. Then we got Fig 10.

The second wall still couldn't be detected in ALOS PALSAR. Firstly, we excluded the possibility of which the second wall was completely disappeared as a result of either natural or man-made destruction, because any effect of corner reflection that formed by wall and earth surface should be detected by SAR with super powerful penetration capability even the second wall was destroyed and completely disappeared from the earth surface. So the reason that the second wall is "disappeared" in ALOS PALSAR image is mostly caused by the imaging parameters of ALOS PALSAR different from SIR-C's.

a SIR-C

b ALOS Palsar

Fig.10 the image of SIR-C and ALOS Palsar after unifying the same resolution and the same distribution scope of gray value

Because the flying orientation of two SAR sensors is very close, we exclude the reason caused by their different direction of view.

There are four prime imaging parameters affect radar return; they are band, polarization, incidence, and direction of view. But according to above parameters' introduction about SIR-C and ALOS PALSAR, only different incidence and direction of view between SIR-C and ALOS PALSAR could result in above phenomena.

And we all know that the incidence is smaller, radar return is stronger. At the same time, we found the maximal incidence of SIR-C is still much smaller than the center incidence of ALOS PALSAR. So their different incidence may be the main reason which result in the second wall was "disappeared" in ALOS PALSAR. Of course, it may be caused by some other system parameters of SIR-C and ALOS sensor, so we need more ALOS PALSAR data and

more integrated experiment that synchronize satellite experiment with ground experiment.

6. LAND COVER CHARACTERIZATION AND CLASSIFICATION USING POLARIMETRIC ALOS PALSAR

Terrain and land cover classification is one of the most important applications of polarimetric synthetic aperture radar(POLSAR) sensing. The objective of the incoherent target decomposition theory is to express the average scattering mechanism as the sum of independent elements in order to associate a physical mechanism with each-component. Polarimetric SAR target decomposition model permits the extraction of target characteristic information, for example, Cloude-Pottier polarimetric target decomposition is presently the most used method for decomposition of natural extended target scattering, from the characteristic decomposition of Hermitian target coherency matrix and α - β model introduced by Cloude and Pottier, some key parameters, such as α -scattering type parameter, H - coherency entropy, A - anistropy, target orientation angle β , target phase angle Φ_i ($i = 1,2,3$) etc have been obtained, the most used parameters are H and α that leads to most popular approach H/α for target scattering classification.

Recently, some new some concerns have been raised with regard to the Cloude-Pottier decomposition. Cloude Alpha's scattering type ambiguities may occur for certain scatters; and certain Cloude-Pottier's parameters like β and the target-phase angles Φ_i may not be roll-invariant for asymmetric targets. A new roll invariant target scattering decomposition, the Touzi target scattering decomposition has been recently introduced. In contrast to the Cloude-Pottier decomposition, the scattering type was introduced as a complex entity in term of the symmetric scattering type magnitude α_s and phase Φ_{α_s}. The new decomposition uses the target helicity τ_m to asses the symmetric nature of targets. So in this study, from the ALOS/PALSAR polarimetric data, the land cover characteristics and classification potential are investigated using these two decomposition models, At last, the conventional polarimetric descriminators are also tested to assess target information that may not be retrieved with the two target scattering decompositions.

Study area locates at the Weinan region of Shan'xi province, in China. The centre latitude /longitude of PALSAR scene is 34° 48′ 23″ N and 109° 28′ 15″ , this region is one of the most important agriculture areas in Shan'xi province. One ALOS/PALSAR polarimetric data scenes has been acquired, the acquisition date are September 4, 2006. To analyze and validate the result, one Landsat TM image acquired at August, 9, 2006 is collected. Fig.11 is the HH backscattering image of study area, Fig.12 is the TM image of study area on 9, August, 2006. The Wei river cross this area from north to south in the left side of image; in the middle of image, there have two large reservoir. During this period, the main land covers of this area are autumn corps (such as corn, potato, cotton and vegetables etc.), fruit trees (such as apple and pear trees etc), forest (mainly locates at mountain area in the right side of image), shrubs, bare soil field, urban, river etc.

Fig.13 is the entropy image of test site derived from $\alpha - \beta$ or Touzi scattering vector model, high entropy mainly corresponds to crops area and forest area located at the mountain area in the right side of image. Fig.14 is the τ_m image derived from the roll-invariant scattering vector model. This parameter is used to assess the symmetric nature of targets, from Fig.14, it can be seen that the τ_m of the most of test area is around the zero, so we can say that the most of target of test site have reflect symmetry property, but, in some area, especially for rectangle area A, B and C, the absolute value of τ_m is larger than that of the most of area, so, these natural targets presents the asymmetric property mainly caused by terrain relief and heterogeneous mixed distribution of bare soil and vegetation etc.

Fig.15 shows the Alpha image derived from $\alpha - \beta$ model, and Fig.16 shows the symmetric scattering type magnitude, α_s , image obtained from the Touzi roll-invariant scattering vector model, the τ_m image shown at Fig.14 will be combined to explain the result difference between Fig.15 and Fig.16. From the Figure, it can be seen that the result are identical for area that τ_m is around zero, for example, in the city area, reservoir area and bare soil area. At the area that τ_m presents large value, the difference between α and α_s is significant, and α is the function of α_s and Φ_{α_s}. For example, for rectangle area A, B, C and the bottom area of the image, the most of them corresponds to terrain relief or heterogeneous area of mixed vegetation and bare soil so that the reflect symmetry property of the targets is damaged.

From physical viewpoints, the Φ_{α_s} is the phase difference between the vector components in the trihedral-dihedral basis, this parameter is polarization basis invariant, and also invariant under a change of antenna wave polarization basis. When target is symmetric scatter, this parameter is identical to the phase difference $\phi_2 - \phi_1$ derived from the $\alpha - \beta$ model. Furthermore, for azimuthally symmetric natural targets, this parameter was interpreted as a measure of relative magnitude of HH and VV, which may be used to separate the Bragg surface from multiple scattering mechanisms. But, in the $\alpha - \beta$ model, this parameter is not used for scattering type

identification because it is not roll invariant. For symmetric target, the information provided by this parameter will significantly improve scattering classification.

Classification Potential Study of Roll-invariant target scattering decomposition

Based on TM image, the classification potential of Touzi scattering vector decomposition model is investigated and validated. From the Fig.17 (a), it can be seen that the result of supervised classification map from entropy and alphas angle is better than that of entropy and alpha angle. For example, for city and farmer residence area and crop area, the classification result of entropy and alphas is better. In the classification map, the river and reservoir are not correctly identified; the reason is not clear at current time because the interval of acquisition time is more than one month between SAR image and TM image. Maybe, in September, the water level of river and reservoir is low or dry.

Fig.18 (a) is the supervised classification map using entropy, alphas and τ_m, it is better than Fig.17 (a). The main reason is that the most of target has quasi symmetry property, so the dynamic range of τ_m is small, and this is not good for target identification. Fig.18 (b) is the supervised classification map using τ_m, alphas and Φ_{α_s}, it can be seen that the result is worst compared with above all result because the city area and framer residence area is poorly classified. From above analysis, we can conclude that the parameters derived from the Touzi scattering vector model can be effectively used for land cover classification, furthermore, the classification result for the combination of entropy, alphas and Φ_{α_s} is the best one.

From the parameters derived from Touzi scattering vector model, the land cover characteristics are compared and discussed, and the potential for these parameters used for land cover classification is investigated. At last, using these parameters and maximum likelihood supervised classification, the classification experimental are implemented, the result indicates that the parameters obtained from Touzi decomposition model can be effectively used for land cover classification, and the classification result for the combination of entropy, alphas and is best one.

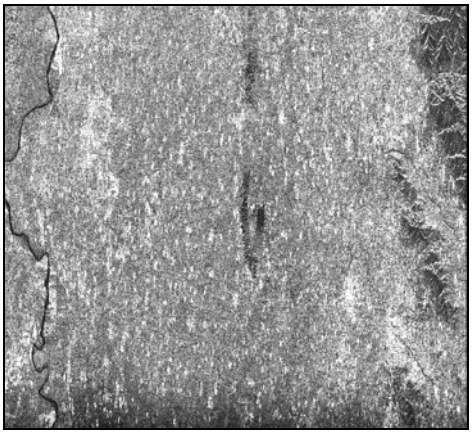

Fig.11 HH backscattering image of study area

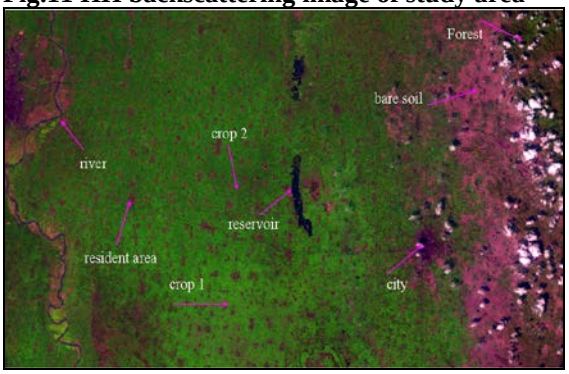

Fig.12 TM image of study area on 9, August, 2006

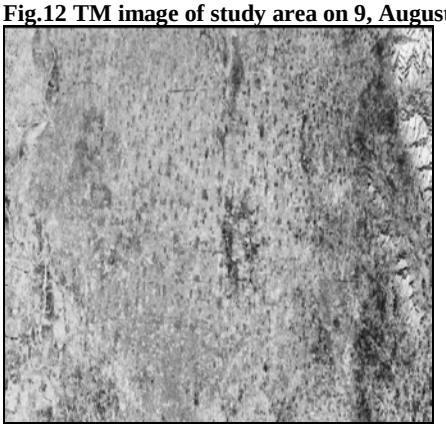

Fig.13 the entropy image of ALOS/PALSAR data

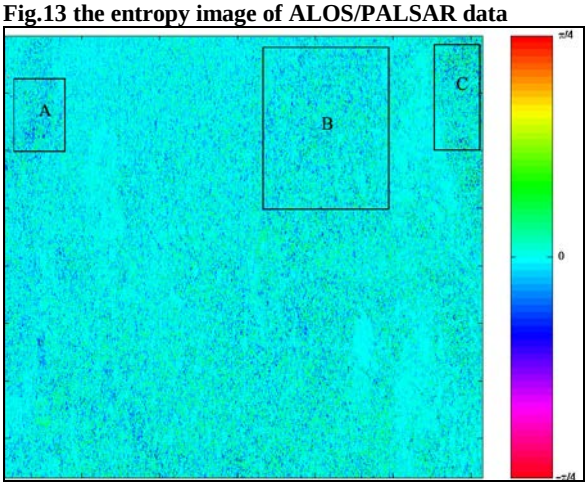

Fig.14 The τ_m image derived from the roll-invariant model

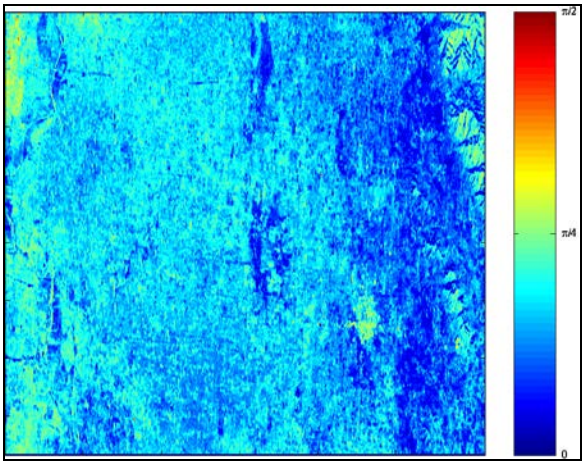

Fig.15 Alpha image derived from $\alpha - \beta$ model

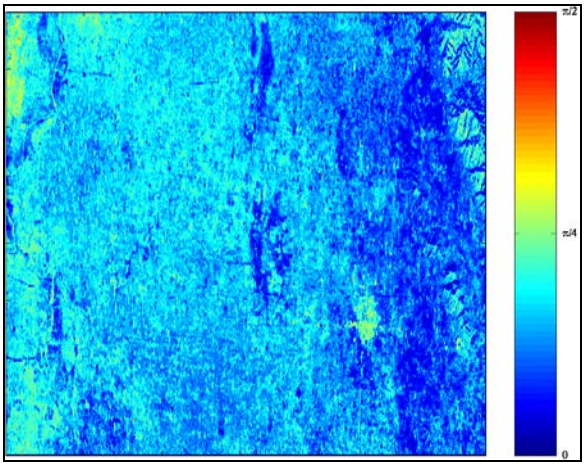

Fig.16 Alphas image derived from Touzi scattering vector model

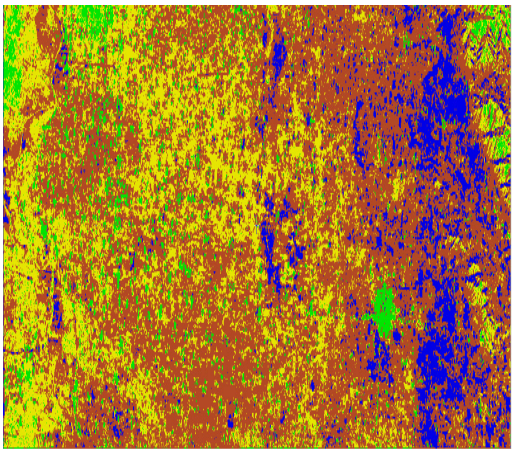

Fig.17(a) The supervised classification map using entropy and alphas angle

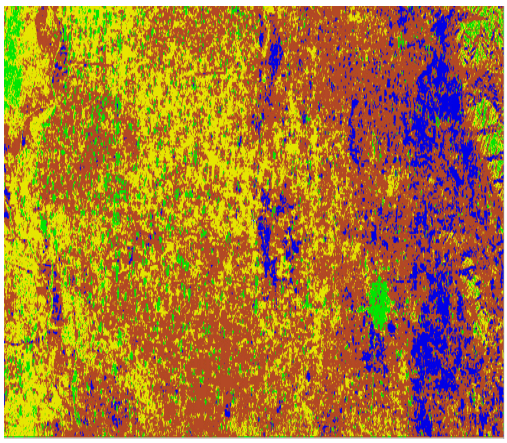

Fig.17 (b) The supervised classification map using entropy, alphas angle and Φ_{α_s} angle

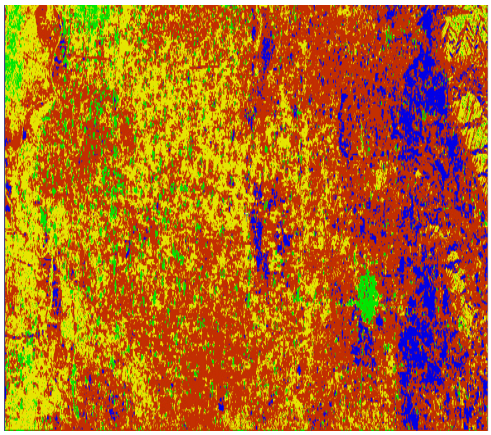

Fig.18(a) The supervised classification map using entropy, alphas angle and τ_m

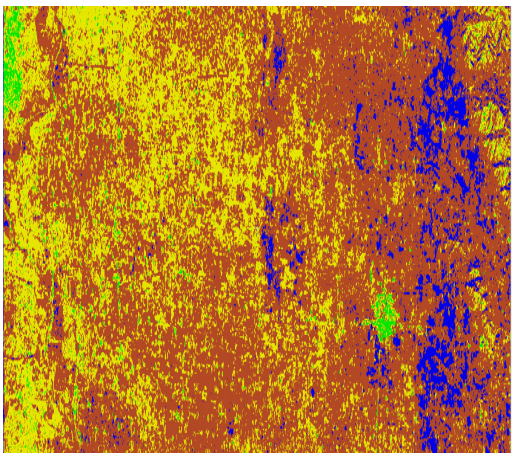

Fig.18 (b) The supervised classification map using τ_m, alphas angle and Φ_{α_s} angle.

Surface roughness parameters and soil moisture retrieve method design and test.

The surface parameters such as surface roughness parameters and soil moisture content are important factors in RADAR science, especially in bare soils. In order to retrieve related parameters mentioned above, we apply the

Genetic Algorithm in the inversion of surface parameters. The study area, Ejin Banner, lies in the west of Nei Monggol altiplano, it mainly consists of desert and Gobi landscape, the famous Ejin oasis is located in the lower reaches of the Heihe River.

When the satellite passed, we measured the field surface parameters, because this area belongs to very arid areas, we only measured the roughness parameters. The next section describes the field surface results measured, RADAR images adopted and the results inverted.

Fig.19 displays the gravels of this area. From Fig.19, we can see the different dimension of the gravels. The surface type of this area is typical of desert and Gobi, and the terrain is relatively flat, so the surface root mean square of surface height (RMSH) is not big, nevertheless, in the different part of the study area, the gravels in scale are different. Fig. 20 displays the instrument for measuring roughness parameters, and the Fig. 21 shows the plot of the samples. When we measured the roughness parameters, we got three to five pictures for each sample point. We considered the averaged value as the final result when dealing with these pictures.

Figure 22 demonstrates the ALOS PALSAR images, which includes HH and HV polarization image. By comparing the two images, we find the PALSAR image may have errors in HV polarization, which will induce errors when retrieving surface parameters.

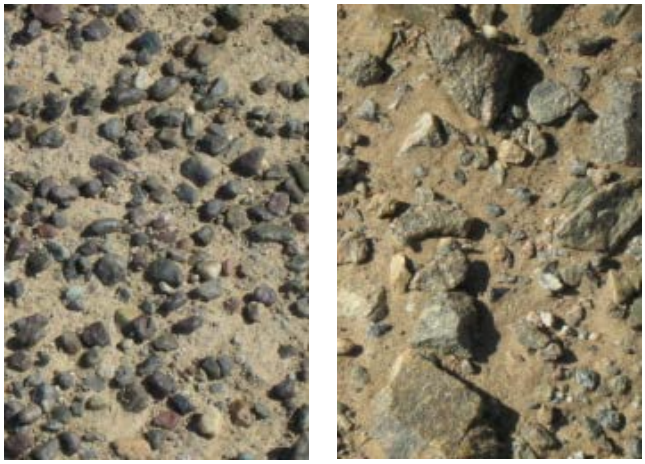

Fig. 19 the gravels of different dimension

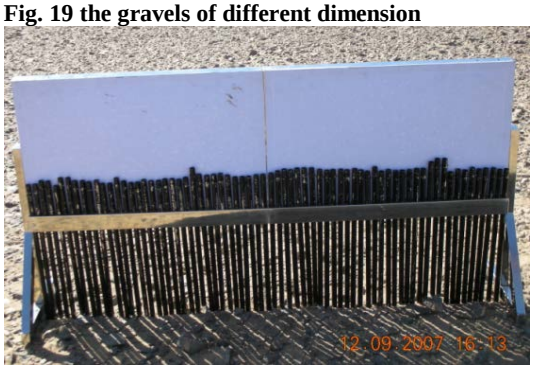

Fig. 20 the instrument for measuring surface roughness parameters

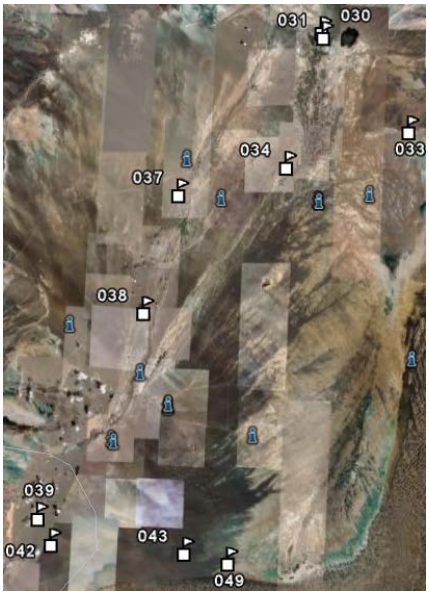

Fig. 21 the plot of samples in 2007

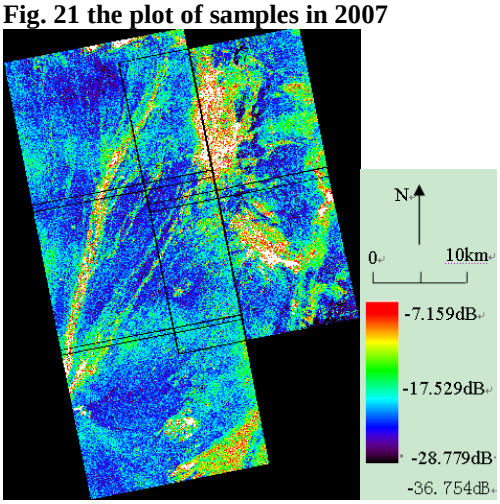

(a) ALOS PALSAR HH

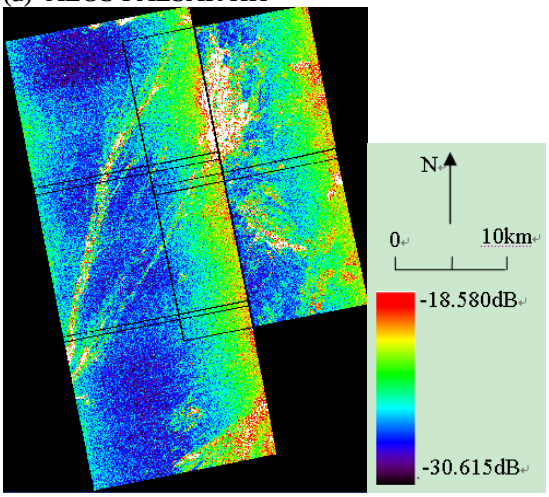

(b) ALOS PALSAR HV

Fig.22 the RADAR backscattering coefficients of ALOS PALSAR

We apply the Genetic Algorithm in the inversion of the surface parameters, the inverted parameters are RMSH、

Correlation Length and the Soil moisture content (in volume). The cost function is designed as:

$$F = 1 \Big/ (1 + \sum | \sigma^0_{pq}\_real(i,j,k) - \sigma^0_{pq}\_theory(i,j,k) |)$$

$$i = 1、2 \cdots n1,\ j = 1、2 \cdots n2, k = 1、2 \cdots n3$$

F denotes the cost function, p and q means the polarization, real and theory means the backscattering coefficient from RADAR images and model, i、j and k means RADAR band、the incidence angle and the type of polarization, n1、n2 and n3 means the total numbers.

Firstly, we attained the backscattering coefficients and incidence angle of each sample point by comparing between the geographical locations ordinates from the RADAR images and the GPS receiver, because the samples mainly lie in the areas covered by ALOS PALSAR images, we mainly used the data from PALSAR; secondly, we retrieved the surface parameters using the genetic algorithm. The retrieval method needs the backscattering coefficients from backscattering model, we adopted two models to testify the precision, one is AIEM model, and another one is the Oh model.

From the comparison between the field measured values and inverted values, we conclude that this inversion method is efficient. At the same time, the PALSAR image in HV polarization may have errors, which may induce unknown errors when retrieving surface parameters. So, we hope the quality of the HV polarization image is improved in the future.

CONCLUSION

The report give some results and show the great potential of ALOS PALSAR data in land surface change monitoring such as glacier movement, Surface roughness parameters, earthquake and etc… since its long bandwidth it could preserve high coherence in mountain area, this could be better for C band SAR sensor, and with the multi-polarization, we could got more information. And we believe that the next generation ALOS-2 could bring more powerful energy for earth observation.

ACKNOWLEDGEMENT

Thanks JAXA for data providing, and thanks other personal that invent the algorithms that used in this paper.

REFERENCE

Burgmann, R., Rosen, P. A., & Fielding, E. J.. Synthetic aperture radar interferometry to measure Earth's surface topography and its deformation. Annual Review of Earth and Planetary Sciences, 28, 169−209,2000

Chen, C. W., & Zebker, H. A. (2002). Phase unwrapping for large SAR interferograms: Statistical segmentation and generalized network models. IEEE Transactions on Geoscience and Remote Sensing, 40, 1709−1719.

Cloude S R and Pottier E. (1996). A review of target decomposition theorems in radar polarimetry. IEEE Transactions on Geoscience and Remote Sensing. 34(2): 498-518.

Curlander, J., and R. McDonough, Synthetic aperture radar systems and signal processing, New York: John Wiley & Sons. 1991.

Fielding, E. J., Wright, T. J., Muller, J., Parsons, B. E., & Walker, R. A seismic deformation of a fold-and-thrust belt imaged by synthetic aperture radar interferometry near Shahdad, Southeast Iran. Geology, 7, 577−580. 2004.

Freeman A and Durden S L. (1998). A three-component scattering model for polarimetric sar data. IEEE Transactions on Geoscience and Remote Sensing 36(3): 963-973.

Massonnet, D., Feigl, K.L., 1998. Radar interferometry and its application to changes in the earth's surface. Reviews of Geophysics 36, 441–500.

Schuler D L, J S Lee, Kasilingam D and Nesti G. (2002). Surface Roughenss and Slope Measurements Using Polarimetric SAR Data. IEEE Transactions on Geoscience and Remote Sensing, 40(3):687-698.

Touzi R, Goze S, Toan T L and Mougin E. (1992). Polarimetric Discriminators for Sar Images. IEEE Transactions on Geoscience and Remote Sensing, 30(5): 973-980.

Touzi R.(2007). Target Scattering Decomposition in Terms of Roll-Invariant Target Parameters. IEEE Transactions on Geoscience and Remote Sensing, 45(1): 73-84.

Yamaguchi Y, Moriyama T, Ishido M and Yamada H. (2005). Four-component scattering model for polarimetric SAR image decomposition. IEEE Transactions on Geoscience and Remote Sensing, 43(8): 1699-1706.

Table II. list of Co-Investigators

Name	E-Mail
Wang ChangLin	wcl_irsa@163.com
Li XinWu	xinwuli@irsa.ac.cn
Liu Guang Corr. Author	liug@tsinghua.org.cn
Zhang Lu	zhanglu0008@163.com
Zhu LanWei	zhulanwei@yahoo.com.cn
Yang huaining	huainingy@126.com
Yan shiyong	yanshiyong@gmail.com
Ruan zhixin	zhixing_ruan@mail.bnu.edu.cn